Available online at www.sciencedirect.com
ScienceDirect
Trans. Nonferrous Met. Soc. China 26(2016) 2874−2882
Transactions of Nonferrous Metals Society of China
www.tnmsc.cn

Hot deformation behavior and microstructural evolution of beta C titanium alloy in β phase field

Xin XU, Li-min DONG, Hong-bo BA, Zhi-qiang ZHANG, Rui YANG

Institute of Metal Research, Chinese Academy of Sciences, Shenyang 110016, China

Received 26 October 2015; accepted 4 May 2016

Abstract: The hot deformation behavior of beta C titanium alloy in β phase field was investigated by isothermal compression tests on a Gleeble−3800 thermomechanical simulator. The constitutive equation describing the hot deformation behavior was obtained and a processing map was established at the true strain of 0.7. The microstructure was characterized by optical microscopy (OM), scanning electron microscopy (SEM) and electron back-scattered diffraction (EBSD) technique. The results show that the flow stress increases with increasing strain rates, and decreases with increasing experimental temperatures. The calculated apparent activation energy (167 kJ/mol) is close to that of self-diffusion in β titanium. The processing map and microstructure observation exhibit a dynamic recrystallization domain in the temperature range of 900−1000 °C and strain rate range of 0.1−1 s^{-1}. An instability region exists when the strain rate is higher than 1.7 s^{-1}. The microstructure of beta C titanium alloy can be optimized by proper heat treatments after the deformation in the dynamic recrystallization domain.

Key words: titanium alloy; hot deformation; dynamic recrystallization; processing map

1 Introduction

Beta C titanium alloy (Ti−3Al−8V−6Cr−4Mo−4Zr) is a metastable β alloy which can be solution treated and aged to achieve a very high ultimate strength of about 1500 MPa [1,2]. After proper heat treatments, beta C titanium alloy can possess a combination of high tensile strength, good ductility, fatigue strength and toughness. Meanwhile, beta C titanium alloy exhibits good hardenability, excellent corrosion resistance and can be cold-worked. Therefore, it can be applied to aerocraft springs, fasteners, deep-sea cables in oceanographic surveys, gas and petroleum piping systems [3−5]. These lead to a great interest in beta C titanium alloy in both technical and academic communities. SCHMIDT et al [1] and EL-CHAIKH et al [2] studied the effect of duplex aging on the fatigue properties of beta C titanium alloy. They found that homogeneous dense precipitates of α phase can be obtained by carefully choosing solution and pre-aging conditions, which benefits the fatigue properties of this alloy. SOMERDAY and GANGLOFF [6] investigated the environment-assisted cracking resistances of beta C titanium alloy with different microstructures, and showed that cold-worked beta C titanium alloy with single β phase and shortly aged beta C titanium alloy with β/α microstructure have enhanced resistance to environment-assisted cracking in aqueous NaCl. GAUDETT and SCULLY [7] reported that this alloy with only solution treatments has lower hydrogen embrittlement susceptibility than that with both solution and aging treatments. RHODES and PATON [8] claimed that beta C titanium alloy possesses the best combination of strength and ductility when the microstructure consists of large non-coherent α phase and β matrix. The ordering behavior and superplasticity of beta C titanium alloy have been also studied [9,10]. ŁUKASZEK-SOŁEK and KRAWCZYK [11] studied the hot deformation behavior of the alloy with the initial microstructure consisting of α and β phases. They obtained the processing, microstructural changes and hardness maps by the dynamic material model (DMM) [12,13]. XU et al [14] studied the effect of different strains on hot deformation behavior of beta C titanium alloy. They observed that abnormal coarse grains have been formed when the strain reached 1.2 at the temperature of 950 °C and strain rate of 1 s^{-1}. Nevertheless, except for the above work, few other papers have discussed the hot deformation behavior of beta C titanium alloy. Despite the lack of investigation,

Corresponding author: Li-ming DONG; Tel: +86-24-23971942; Fax: +86-24-23902021; E-mail: lmdong@imr.ac.cn
DOI: 10.1016/S1003-6326(16)64416-3

hot deformation is an important process for the manufacture of beta C titanium alloy. There are two major purposes for hot deformation [15], i.e., producing finished shapes of products, and improving mechanical properties of materials by controlling microstructure during different stages of hot deformation. The microstructure after hot deformation has great influences on both subsequent processes of semi-products and the performance of final products [13]. Therefore, it is of profound importance to investigate the hot deformation behavior of beta C titanium alloy in order to optimize the processing and improve its properties and applications. Moreover, alloys with different processing history and initial microstructures show different hot deformation behaviors [16]. Hence, an initial microstructure different from previous studies was adopted in this work. In addition, the constitutive analysis and processing maps based on DMM have been extensively used to study the hot workability of various alloys, e.g., magnesium alloys [17−19], superalloys [20−22], aluminum alloys [23,24], steels [25−27] and titanium alloys [11,15,16,28−31]. These investigations have shown that the constitutive analysis and processing maps have good capacity for determining hot deformation mechanisms and predicting microstructural evolution. Therefore, in this study, isothermal compression tests have been conducted on beta C titanium alloy in β phase field. The object of this study is to investigate the mechanisms of hot deformation and optimal processing conditions of beta C titanium alloy in β phase field based on the constitutive equation, processing map and microstructural observations.

2 Experimental

Beta C titanium alloy bar with the diameter of 6 mm was used in this study; its composition is shown in Table 1. The β transus is about 750 °C measured by the metallographic method. The initial microstructure consists of equiaxed β grains of 20−30 μm in diameter, as shown in Fig. 1. Cylindrical compression samples were machined to 6 mm in diameter and 9 mm in height.

Table 1 Chemical composition of beta C titanium alloy used in this experiment (mass fraction, %)

Al	V	Cr	Mo	Zr	C	O	N	H	Ti
3.46	8.08	6.04	3.94	3.92	0.02	0.10	0.014	0.001	Bal.

All the isothermal compression tests were carried out on a Gleeble−3800 thermomechanical simulator. The temperature range was 800−1000 °C with 50 °C intervals and the strain rate range was 0.001−10 s^{-1}. After being heated to the deformation temperature with a heating rate of 5 °C/s, samples were soaked for 2 min and then compressed by 60% height reduction (true strain ε=0.9). The deformed samples were air-cooled to room temperature. In order to measure the instantaneous temperature, thermocouples were welded on the middle surface of samples. The ends of samples were coated with lubricant consisting of high quality nickel powder and graphite. Tantalum foils were placed between the ends and the rams to reduce the friction and obtain uniform deformation. The deformed samples were sectioned parallel to the compression axis and prepared for metallographic examinations using standard techniques. Microstructure observations were carried out using a ZEISS Axiovert 200MAT OM and a SHIMADZU SSX−550 SEM. EBSD analysis was conducted on a HITACHI S−3400N SEM with the HKL-CHANNEL 5 analysis package.

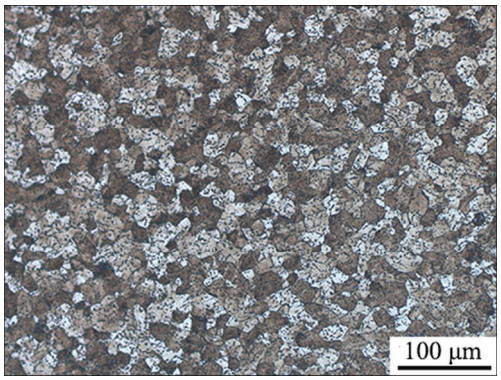

Fig. 1 Initial microstructure of beta C titanium alloy used in this study

3 Results and discussion

3.1 Stress−strain behavior

The true strain−true stress curves of beta C titanium alloy deformed at 800 and 1000 °C are shown in Fig. 2. The true strain−true stress curves under other conditions show the similar features with them. The flow stress increases with the increase of strain rates and the decrease of experimental temperatures. When the strain rate is 10 s^{-1}, the stress reaches a high level at low strain and the curves reveal slight strain hardening followed by continuous flow softening. At the end, flow stresses achieve the steady state.

The extent of the flow softening decreases with increasing experimental temperature. One mechanism of flow softening is suggested to be deformation heating [28]. The real temperature of samples increases (Table 2) because the deformation heating cannot be conducted to surroundings in time due to the short deformation time and the low thermal conductivity of titanium alloys. With increasing temperature, atom diffusion and dislocation movements occur more easily, which causes the flow

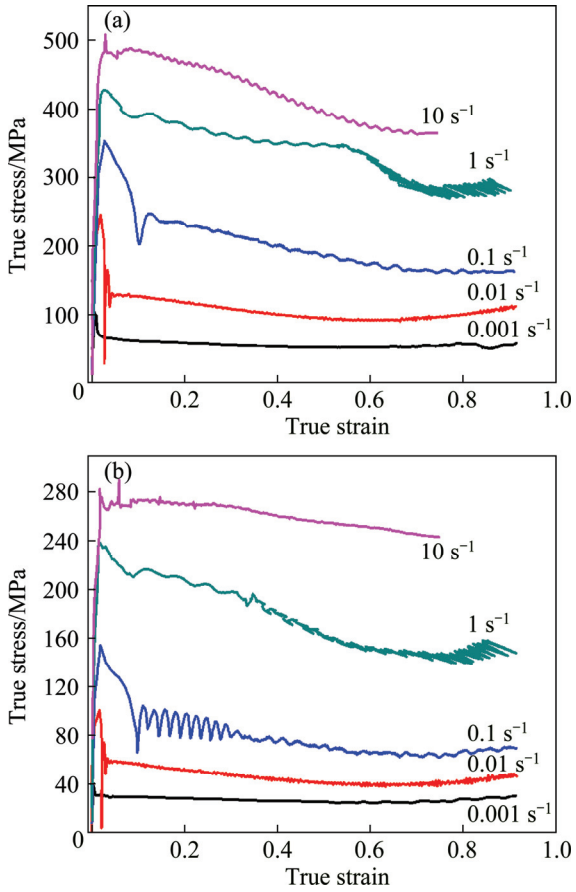

Fig. 2 Flow curves of beta C titanium alloy deformed at 800 °C (a) and 1000 °C (b)

Table 2 Temperature difference between instantaneous temperature and experimental temperature of beta C titanium alloy under different deformation conditions

Temperature/ °C	Strain rate/s^{-1}	Temperature difference/°C			
		ε=0.3	ε=0.5	ε=0.6	ε=0.7
800	0.1	−1	−2	−2	−3
	1	18	3	−6	−8
	10	23	38	43	46
850	0.1	−2	−2	−2	−3
	1	11	−5	−6	−4
	10	23	30	35	39
900	0.1	−1	−2	−2	−3
	1	8	−10	−5	−3
	10	18	29	33	36
950	0.1	−3	−3	−3	−3
	1	−1	−8	−8	−9
	10	12	19	22	23
1000	0.1	−1	−2	−3	−3
	1	3	−5	−5	−6
	10	16	22	24	25

The temperature differences for other conditions are zero.

stress to decrease. Meanwhile, when compression reaches adiabatic conditions, adiabatic heating can cause flow localization leading to flow instability. In addition, superplasticity, dynamic recovery (DRV) and dynamic recrystallization (DRX) can also cause softening [30,31].

When the strain rate is below 10 s^{-1}, all curves show that flow stresses increase rapidly and reach peak stresses at a small strain level (<0.03) and then drop sharply. These are due to discontinuous yielding phenomenon which has been observed in a great number of β titanium alloys [15]. The extensively accepted mechanism for this phenomenon is the dynamic theory which associates discontinuous yielding with the rapid generation and multiplication of new mobile dislocations. This starts at grain boundary sources and is then transmitted to grain interiors [29,32]. At constant temperatures, the yielding drop increases with the increase of strain rates from 0.001 to 0.1 s^{-1} and reaches the greatest drop at 0.1 s^{-1}, then decreases when strain rates are faster than 0.1 s^{-1}. In this study, it is also found that increments of experimental temperatures result in decrements of yielding drops at a constant strain rate. It can be concluded that the discontinuous yielding drop is a function of temperature and strain rate. This agrees with previous studies [32].

After the discontinuous yielding, all the curves, except for the one of 0.001 s^{-1}, show flow softening. However, the flow softening has accelerated periods in certain true strain ranges, e.g., 0.55−0.65 at 800 °C, 0.4−0.6 at 1000 °C, before a steady-state type flow behavior when the strain rate is 1 s^{-1}. During the accelerating period the instantaneous temperature of samples is lower than the experimental temperature (Table 2), which intensifies the work hardening. Therefore, the apparent softening acceleration indicates that the softening processes in the samples are more intensified than the work hardening. XU et al [14] have studied the effect of strain on hot deformation behavior of beta C titanium alloy. They suggested that the apparent softening acceleration is because of the fierce microstructural evolution which consumes power and reduces the dislocation density of matrices [14]. When strain rates are 0.1 s^{-1} and 0.01 s^{-1}, the flow curves reach the steady state after a long period of slight flow softening and show slight hardening at the end. Moreover, the curves show different extents of oscillations (Fig. 2) when strain rates are higher than 0.01 s^{-1}. Mechanisms for the phenomenon may be DRX, flow instability or micro-cracking [30]. When the strain rate is 0.001 s^{-1}, the curves are of steady-state types indicating that the softening like superplasticity, DRV or DRX is sufficiently fast to balance the rate of work hardening.

3.2 Kinetic analysis

The relationship among flow stress σ, strain rate $\dot{\varepsilon}$ and deformation temperature T during hot deformation is generally described as a constitutive equation [13,18,30,31]:

$$\dot{\varepsilon} = A\sigma^n \exp(-\frac{Q}{RT}) \quad (1)$$

where Q is the apparent activation energy, R is the mole gas constant, n is the stress exponent and A is the material constant. In order to determine the constitutive equation and analyze the mechanisms of hot deformation, n and Q were calculated. Steady-state stresses (corresponding to ε=0.7) were used as σ. From Eq. (1), the stress exponent, n, is defined by

$$n=\left(\frac{\partial \ln \dot{\varepsilon}}{\partial \ln \sigma}\right)_T \quad (2)$$

and the activation energy, Q, is defined by

$$Q=\left(\frac{nR\partial \ln \sigma}{\partial(1/T)}\right)_{\dot{\varepsilon}} \quad (3)$$

The values of n and Q can be computed from the plots of $\ln \dot{\varepsilon}$ vs $\ln \sigma$ and $1000/T$ vs $\ln \sigma$ (Fig. 3). Figure 3 was plotted using the linear regression fit. The stress exponent is estimated to be 4.1 and Q for beta C titanium alloy is calculated to be 167 kJ/mol. It has been reported that Q of hot deformation for beta titanium alloys was in the range of 130−183 kJ/mol [15, 33]. Q calculated in this work is within the reported range. It is very close to the activation energy for self-diffusion in β titanium (153 kJ/mol [34]), so it is reasonable to consider the dislocation climb as the main deformation mechanism [34,35]. In some reports, this is believed to imply that DRV is the rate controlling mechanism in β phase field [15,35]. However, taking the large strain into consideration, recrystallization or selective recrystallization may occur and DRX has been found during deformation in β phase field when the deformation temperature is above $0.8T_m$ (T_m is the melting point) [33]. Furthermore, beta C titanium alloy has a high content of alloying elements which can provide nuclei for DRX. Therefore, further investigations are needed to determine the microstructural evolution mechanisms.

The combined influences of strain rate and deformation temperature on hot working process can be evaluated by Zener−Hollomom constant Z which is also used to assess the validity of the constitutive equation [23,29]. Z is a temperature compensated strain rate parameter defined by

$$Z = \dot{\varepsilon} \exp(\frac{Q}{RT}) \quad (4)$$

The values of Z and steady-state stresses are plotted with a linear regression fit in Fig. 4. It can be seen that

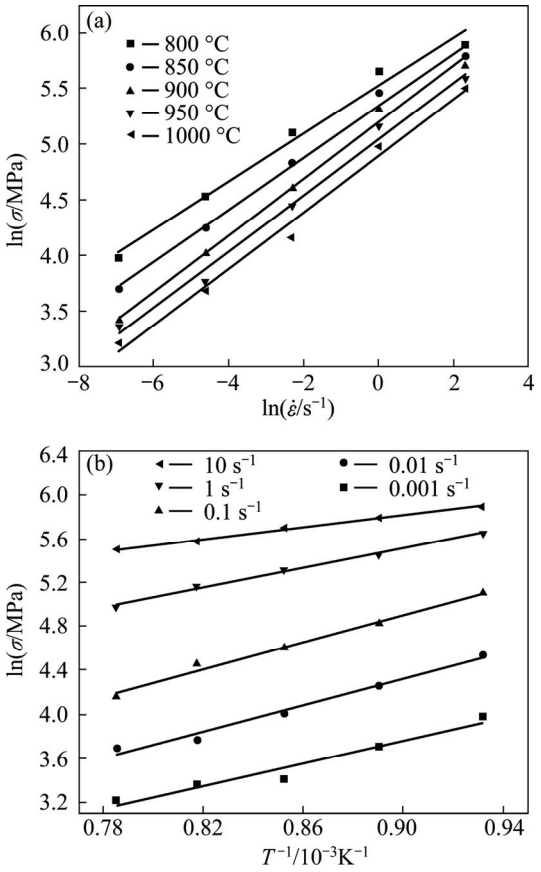

Fig. 3 Plots of $\ln \sigma$ vs $\ln \dot{\varepsilon}$ (a) at various deformation temperatures and $\ln \sigma$ vs T^{-1} (b) with various strain rates

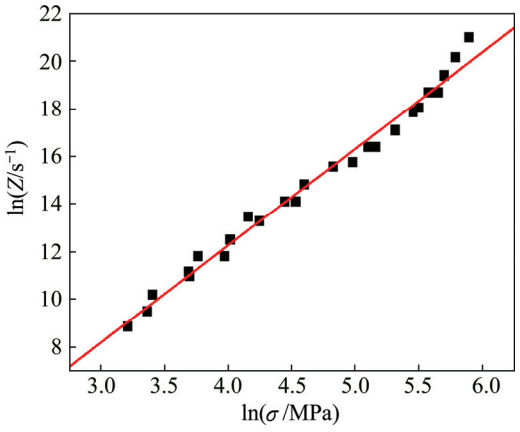

Fig. 4 Plot of Zener−Hollomon parameter with different flow stresses

there is a nice linear relationship between $\ln Z$ and $\ln \sigma$ and the correlation coefficient is 0.99.

From Eqs. (1) and (4), the correlation of Z and σ can be expressed as

$$Z = A\sigma^n \quad (5)$$

Equation (5) is consistent with Fig. 4. The stress exponent given by the slope of the plot is 4.07 which is very close to that given by Fig. 3. The material constant

A can be calculated from Fig. 4 being 1.81×10^{-2}. Based on the above results, the constitutive equation describing the hot deformation behavior of beta C titanium alloy in β phase field is expressed as

$$\dot{\varepsilon}=1.81\times10^{-2}\sigma^{4.07}\exp(\frac{-167000}{RT}) \quad (6)$$

The high correlation coefficient suggests that it is reasonable to use the obtained constitutive equation to describe the hot deformation behavior of beta C titanium alloy in β phase field. Equation (6) may provide the basis for choosing the hot working parameters and numerical simulations of plastic processing of beta C titanium alloy.

3.3 Processing map

On the basis of DMM [12,13], the processing map of beta C titanium alloy at the strain of 0.7 was plotted. In this model, the partitioning between the two parts of powers dissipated as heat through plastic deformation and that dissipated by microstructural evolution is determined by the constitutive flow behavior of materials and calculated by the strain rate sensitivity m which is defined by

$$\frac{\mathrm{d}J}{\mathrm{d}G}\approx\frac{\Delta\lg\sigma}{\Delta\lg\dot{\varepsilon}}=m \quad (7)$$

where G content and J co-content represent the power dissipated by heat and microstructural evolution, respectively. The value of J is normalized with respect to the power dissipation through the microstructure in an ideal dissipater to obtain a dimensionless parameter called the efficiency of power dissipation defined by

$$\eta=\frac{2m}{m+1} \quad (8)$$

Plotting η as a function of strain rate and deformation temperature gives the power dissipation map which indicates the process of microstructural evolution during hot deformation. A continuum criterion for the flow instability is obtained from the principle of the maximum rate of entropy production expressed by

$$\xi(\dot{\varepsilon})=\frac{\partial\ln[m/(m+1)]}{\partial\ln\dot{\varepsilon}}+m<0 \quad (9)$$

where $\xi(\dot{\varepsilon})$ is the instability parameter which is a function of strain rate and deformation temperature. The contours of different ξ with various strain rates and temperatures constitute an instability map. A processing map is produced by superimposing the instability map on the power dissipation map.

The processing map at ε=0.7 is shown in Fig. 5 which is different from the one in Ref. [11] due to different initial microstructures. The microstructural evolution during hot deformation is also different. As can be seen, the instability region (the shadow area) is on the top of the map. When the strain rate is higher than 1.7 s^{-1}, flow instability takes place during hot working over the entire temperature range. At high strain rates, the time for deformation is limited and the deformation heat cannot be conducted to other parts of the sample in time so that the local temperature rises and the flow stress becomes lower, which causes plastic flow to be localized. When adiabatic conditions are satisfied, flow localization bands are generated and flow instabilities occur [30]. This can be illustrated by the microstructural observation as shown in Fig. 6. The flow localization bands at an angle of about 45° to the compression axis can be seen clearly from Fig. 6. In addition, fine grains are formed within the flow localization bands, which makes microstructures inhomogeneous. As shown in

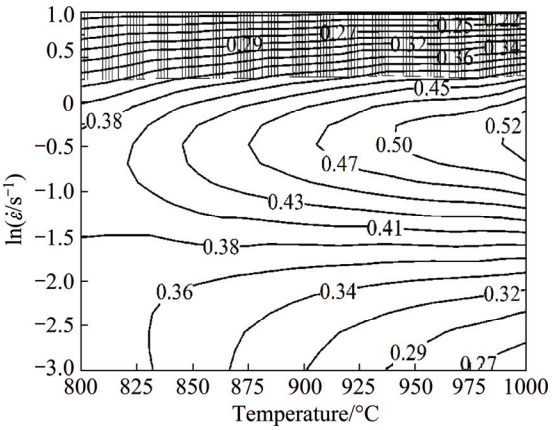

Fig. 5 Processing map for beta C titanium alloy at ε=0.7

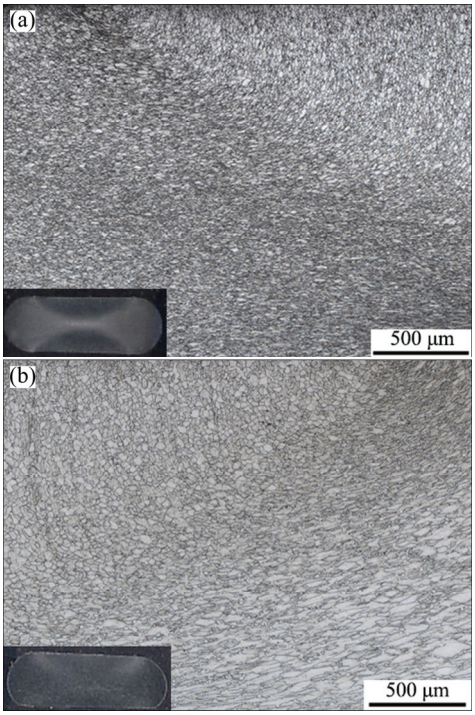

Fig. 6 Macrostructure and microstructure of beta C titanium alloy deformed at 800 °C, 10 s^{-1} (a) and 1000 °C, 10 s^{-1} (b)

Fig. 2, when the strain rate is 10 s^{-1}, flow curves exhibit continuous flow softening. Since there is no sample cracking under tests, and no micro-cracking or voids have been observed, the flow localization is the reason for the instability. During hot working of beta C titanium alloy, the instability region should be avoided.

In the processing map, there is a high efficiency domain (η=47%−52%) in the temperature range of 900−1000 °C and strain rate range 0.1−1 s^{-1} with a peak efficiency of 52%. This domain is associated with DRX of high stacking fault energy materials like BCC metals [29,33]. That is to say, in the above domain, DRX is the dominant mechanism of microstructural evolution in this study. For other domains, the efficiency of power dissipation is lower, indicating that DRV is the main mechanism under these conditions. DRX is beneficial to hot workability since it can refine microstructure and lower flow stresses. Therefore, it is safe to hot work beta C titanium alloy in the DRX domain and the optimum condition is suggested to be 1000 °C and 0.5 s^{-1} according to the processing map.

3.4 Microstructural observation

Figure 7 shows the typical microstructures of deformed samples. After deformation, prior β grains are elongated transversely to the compression axis. Prior β grains become coarser with increasing temperature at constant strain rates. At constant temperatures, the prior β grains become thinner with the increase of strain rate since the compressed prior β grains have less time to grow at higher strain rates. For all conditions, the prior β-grain boundaries are serrated and substructures appear in the interior of elongated prior β grains. These are signatures of DRV. It can be seen that new fine undeformed grains are generated under the conditions of 950−1000 °C, 0.1−1 s^{-1}. This indicates that DRX occurs. These observations are consistent with the processing map analysis. In addition, the new fine grains appear along prior grain boundaries instead of the interior of prior β grains. Moreover, the flow curves under these conditions present oscillation and show multipeak stress values (Fig. 2). These behaviors may imply discontinuous dynamic recrystallization [36]. When the strain rate reaches 0.1−10 s^{-1}, uniform subgrains are formed in some elongated prior β grains and some prior β grains thin down to the width of one to three subgrain at the center of the samples (Fig. 7), which results in geometrical dynamic recrystallization (GDRX) [36]. This may be authenticated by flatter prior β-grain boundaries. At the large strain, the prior β grains become elongated and thin. Meanwhile, grains do not have sufficient time to grow at large strain rates. When the prior β grains are thinned down to the size of three subgrains or even smaller one, serrated grain boundaries on opposite sides may contact, pinching-off the grains and reducing surface energy. As a consequence, the grains are shortened and their neighbors are thickened. This phenomenon is also called grain refining DRV [36]. It should be pointed out that the flow localization has also been observed at 950 °C and 10 s^{-1}, which is not shown in Fig. 7(c) since it just illustrates the very center area of the sample.

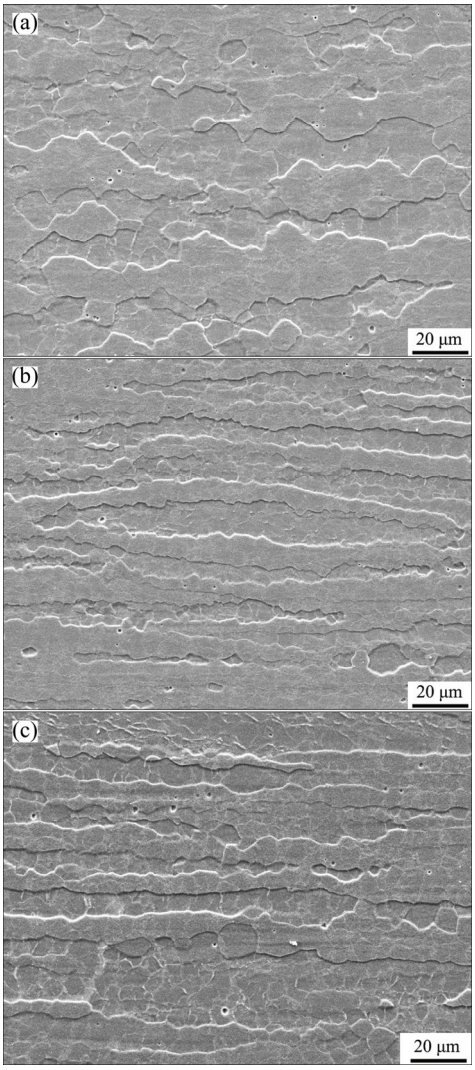

Fig. 7 Microstructures of beta C titanium alloy deformed at 950 °C, 0.1 s^{-1} (a), 950 °C, 1 s^{-1} (b) and 950 °C, 10 s^{-1} (c) showing typical GDRX

Figure 8 shows grain boundary characteristics of deformed beta C titanium alloy obtained by EBSD technique. As shown in Figs. 8(a) and (c), substructures exist in the prior β grains implying the occurrence of DRV. Misorientation angle distribution maps (Figs. 8(b) and (d)) demonstrate clearly that the ratio of high angle boundaries is high at 950 °C, 0.1 s^{-1}, which is evidence of DRX occurrence.

In many cases, hot deformed materials are used as intermediate products for subsequent processes, e.g., heat

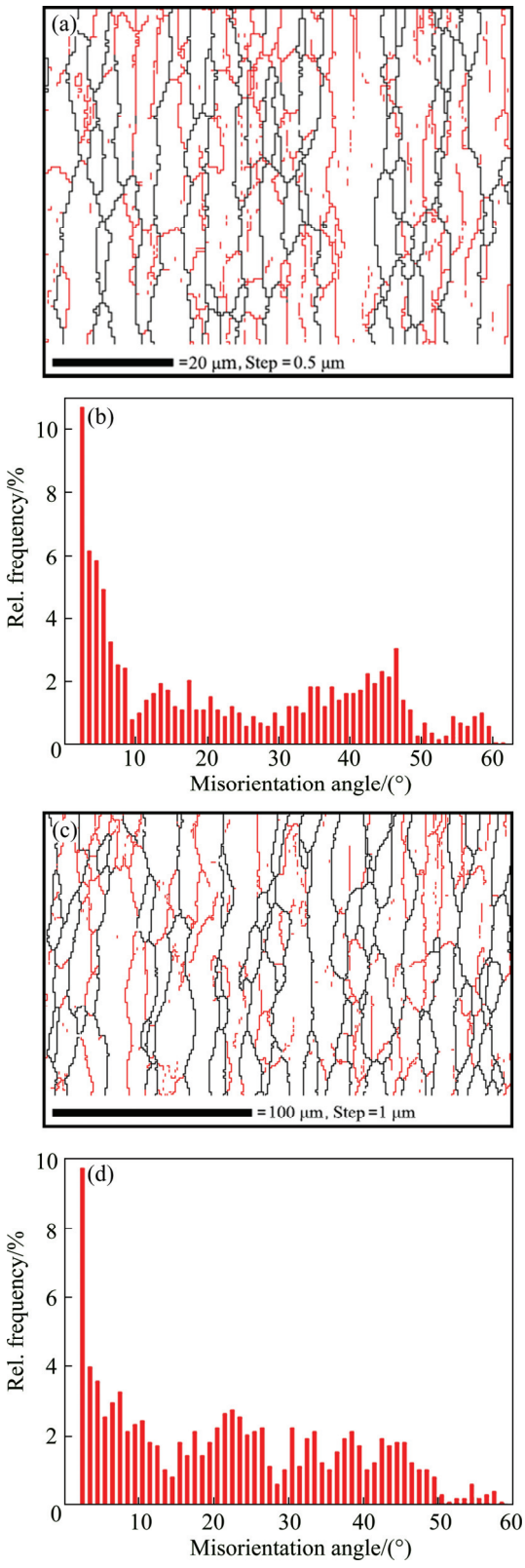

Fig. 8 Grain boundary maps (a) and (c), and corresponding misorientation angle distribution maps (b) and (d) of beta C titanium alloy deformed at 800 °C, 0.1 s^{-1} (a, b) and 950 °C, 0.1 s^{-1} (c, d), respectively (Red lines in (a) and (c) represent low-angle boundaries between 2° and 15° and black lines represent high-angle boundaries higher than 15°)

treatments, before application. In order to examine the effects of hot deformation on the microstructure of beta C titanium alloy during subsequent heat treatments, deformed specimens were heat treated at 800 °C for 70 min and then air cooled. The microstructure after heat treatment is shown in Fig. 9. The microstructure of the specimen deformed at 1000 °C and 0.1 s^{-1} consists of fine grains. The average size of the grains is about 18 μm. It is reasonable to consider that the alloy with this kind of microstructure has excellent properties. By contrast, the grain sizes of specimens deformed at 800 °C, 0.1 s^{-1} and 1000 °C, 0.001 s^{-1} are much thicker. These validate that deformation in the DRX domain obtained in this study will optimize the microstructure of beta C titanium alloy and may result in excellent properties.

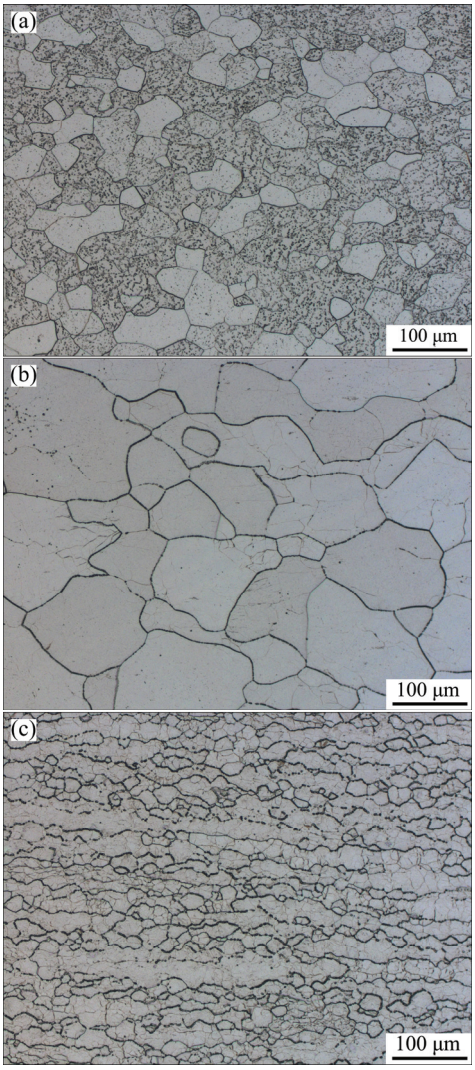

Fig. 9 Microstructure of beta C titanium alloy deformed at 800 °C, 0.1 s^{-1} (a), 1000 °C, 0.001 s^{-1} (b) and 1000 °C, 0.1 s^{-1} (c) after annealing at 800 °C for 70 min and air cooling

4 Conclusions

1) The apparent activation energy was calculated to

be 167 kJ/mol. Constitutive equations are obtained to characterize the hot deformation behavior of beta C titanium alloy in β phase field.

2) In the temperature range of 900−1000 °C and strain rate range of 0.1−1 s^{-1}, DRX is the dominant microstructural evolution mechanism and accompanied with DRV. Under other conditions, the microstructure mainly undergoes DRV. This agrees with the processing map. When the strain rate is 0.1−10 s^{-1}, the GDRX occurs during hot deformation.

3) The microstructure of beta C titanium alloy deformed in the DRX domain obtained and then heat treated at 800 °C for 70 min consists of fine grains which may improve mechanical properties.

References

[1] SCHMIDT P, EL-CHAIKH A, CHRIST H J. Effect of duplex aging on the initiation and propagation of fatigue cracks in the solute-rich metastable β titanium alloy Ti 38-644 [J]. Metallurgical and Materials Transactions A, 2011, 42(9): 2652−2667.

[2] EL-CHAIKH A, SCHMIDT P, CHRIST H J. Fatigue properties of duplex-aged Ti 38-644 metastable beta titanium alloy [J]. Procedia Engineering, 2010, 2(1): 1973−1982.

[3] YAMASHITA Y, TSUCHIYA K, IRIE N, YAMADA N, ISHIOU S, MORLI A, MURAYAMA Y. Manufacturing technology and application of titanium alloy wire rod to deep-sea cable [J]. Nippon Steel Technical Report, 1994, 62: 52−56.

[4] YU K O, CRIST E M, PESA R, CECCHINI N, BUGLE C M. Single-melt beta C for spring and fastener applications [J]. Journal of Materials Engineering and Performance, 2005, 14(6): 697−702.

[5] NYAKANA S L, FANNING J C, BOYER R R. Quick reference guide for β titanium alloys in the oos [J]. Journal of Materials Engineering and Performance, 2005, 14(6): 799−811.

[6] SOMERDAY B P, GANGLOFF R P. Effect of strength on environment-assisted cracking of Ti−8V−6Cr−4Mo−4Zr−3Al in aqueous NaCl. Part 1: Age hardening vs. work hardening [J]. Materials Science and Engineering A, 1998, 254(1): 166−178.

[7] GAUDETT M A, SCULLY J R. Part I—The effects of pre-dissolved hydrogen on cleavage and grain boundary fracture initiation in metastable beta Ti−3Al−8V−6Cr−4Mo−4Zr [J]. Metallurgical and Materials Transactions A, 1999, 30(1): 65−79.

[8] RHODES C G, PATON N E. The influence of microstructure on mechanical properties in Ti−3AI−8V−6Cr−4Mo−4Zr (Beta-C) [J]. Metallurgical Transactions A, 1977, 8(11): 1749−1761.

[9] CHOE B H, LEE B H, LEE J H, LEE T H, LEE C G, KIM S J, LEE Y T. The ordering behavior of supersaturated metastable phases in β-Ti alloys [J]. Metals and Materials International, 2001, 7(6): 551−556.

[10] SALAM A, HAMMOND C. Superplasticity and associated activation energy in Ti−3Al−8V−6Cr−4Mo−4Zr alloy [J]. Journal of Materials Science, 2005, 40(20): 5475−5482.

[11] ŁUKASZEK-SOŁEK A, KRAWCZYK J. The analysis of the hot deformation behaviour of the Ti−3Al−8V−6Cr−4Zr−4Mo alloy, using processing maps, a map of microstructure and of hardness [J]. Materials & Design, 2014, 65: 165−173.

[12] PRASAD Y V R K, GEGEL H L, DORAIVELU S M, MALAS J C, MORGAN J T, LARK K A, BARKER D R. Modelling of dynamic materials behavior in hot deformation: Forging of Ti-6242 [J]. Metallurgical Transactions A, 1984, 15: 1883−1892.

[13] PRASAD Y V R K, RAO K P, SASIDHAR S. Hot working guide: A compendium of processing maps [M]. 2nd ed. Materials Park, Ohio: ASM International, 2015: 2−11.

[14] XU Xin, DONG Li-min, ZHANG Zhi-qiang, BA Hong-bo, HU Ming, GUAN Shao-xuan, YANG Rui. Effect of strain on hot deformation behavior and microstructure of TB9 titanium alloy [J]. The Chinese Journal of Nonferrous Metals, 2013, 23(S): s566−s570. (in Chinese)

[15] WEISS I, SEMIATIN S L. Thermomechanical processing of beta titanium alloys—An overview [J]. Materials Science and Engineering A, 1998, 243(1): 46−65.

[16] LUO Jiao, LI Lian, LI Miao-quan. Deformation behavior of Ti−5Al−2Sn−2Zr−4Mo−4Cr alloy with two initial microstructures during hot working [J]. Transactions of Nonferrous Metals Society of China, 2016, 26(2): 414−422.

[17] SRINIVASAN M, LOGANATHAN C, NARAYANASAMY R, SENTHILKUMAR V, NGUYEN Q B, GUPTA M. Study on hot deformation behavior and microstructure evolution of cast-extruded AZ31B magnesium alloy and nanocomposite using processing map [J]. Materials & Design, 2013, 47(9): 449−455.

[18] GALL S, HUPPMANN M, MAYER H M, MÜLLER S, REIMERS W. Hot working behavior of AZ31 and ME21 magnesium alloys [J]. Journal of Materials Science, 2013, 48(1): 473−480.

[19] LI Ju-qiang, LIU Juan, CUI Zhen-shan. Characterization of hot deformation behavior of extruded ZK60 magnesium alloy using 3D processing maps [J]. Materials & Design, 2014, 56: 889−897.

[20] LU Yan-ling, LIU Jin-xi, LI Xiao-ke, LIANG Jian-ping, LI Zhi-jun, WU Guan-yuan, ZHOU Xing-tai. Hot deformation behavior of Hastelly C276 superalloy [J]. Transactions of Nonferrous Metals Society of China, 2012, 22(S1): s84−s88.

[21] ZHANG Hong-bin, ZHANG Kai-feng, LU Zhen, ZHAO Chang-hong, YANG Xiao-li. Hot deformation behavior and processing map of a γ'-hardened nickel-based superalloy [J]. Materials Science and Engineering A, 2014, 604: 1−8.

[22] JI Ya-qi, QU Shun-de, HAN Wei-xin. Hot deformation and processing map of GH3535 superalloy [J]. Transactions of Nonferrous Metals Society of China, 2015, 25(1): 88−94.

[23] WANG Ming-liang, JIN Pei-peng, WANG Jin-hui, LI Han. Hot deformation behavior of as-quenched 7005 aluminum alloy [J]. Transactions of Nonferrous Metals Society of China, 2014, 24(9): 2796−2804.

[24] ZHANG Tian, TAO You-rui, WANG Xue-yin. Constitutive behavior, microstructural evolution and processing map of extruded Al−1.1Mn−0.3Mg−0.25RE alloy during hot compression [J]. Transactions of Nonferrous Metals Society of China, 2014, 24(5): 1337−1345.

[25] MIRZADEH H, PARSA M H, OHADI D. Hot deformation behavior of austenitic stainless steel for a wide range of initial grain size [J]. Materials Science and Engineering A, 2013, 569: 54−60.

[26] MIRZADEH H, NAJAFIZADEH A. Hot deformation and dynamic recrystallization of 17-4 PH stainless steel [J]. ISIJ International, 2013, 53(4): 680−689.

[27] HAN Ying, LIU Gui-wu, ZOU De-ning, LIU Rong, QIAO Guan-jun. Deformation behavior and microstructural evolution of as-cast 904L austenitic stainless steel during hot compression [J]. Materials Science and Engineering A, 2013, 565: 342−350.

[28] DING R, GUO Z X, WILSON A. Microstructural evolution of a Ti−6Al−4V alloy during thermomechanical processing [J]. Materials Science and Engineering A, 2002, 327(2): 233−245.

[29] FAN Jiang-kun, KOU Hong-chao, LAI Min-jie, TANG Bin, CHANG Hui, LI Jin-shan. Characterization of hot deformation behavior of a new near beta titanium alloy: Ti-7333 [J]. Materials & Design, 2013, 49: 945−952.

[30] SESHACHARYULU T, MEDEIROS S C, FRAZIER W G, PRASAD Y. Hot working of commercial Ti−6Al−4V with an equiaxed α–β microstructure: Materials modeling considerations [J]. Materials

Science and Engineering A, 2000, 284(1): 184−194.
[31] LIANG Hou-quan, GUO Hong-zhen, NAN Yang, QIN Chun, PENG Xiao-na, ZHANG Jing-li. The construction of constitutive model and identification of dynamic softening mechanism of high-temperature deformation of Ti−5Al−5Mo−5V−1Cr−1Fe alloy [J]. Materials Science and Engineering A, 2014, 615: 42−50.
[32] PHILIPPART I, RACK H J. High temperature dynamic yielding in metastable Ti−6.8Mo−4.5F−1.5Al [J]. Materials Science and Engineering A, 1998, 243(1): 196−200.
[33] BALASUBRAHMANYAM V V, PRASAD Y. Deformation behavior of beta titanium alloy Ti−10V−4.5Fe−1.5Al in hot upset forging [J]. Materials Science and Engineering A, 2002, 336(1): 150−158.
[34] DYMENT F, LIBANATI C M. Self-diffusion of Ti, Zr, and Hf in their HCP phases, and diffusion of Nb95 in HCP Zr [J]. Journal of Materials Science, 1968, 3(4): 349−359.
[35] LIU Y, BAKER T N. Deformation characteristics of IMI685 titanium alloy under β isothermal forging solutions [J]. Materials Science and Engineering A, 1995, 197(2): 125−131.
[36] MCQUEEN H J. Development of dynamic recrystallization theory [J]. Materials Science and Engineering A, 2004, 387: 203−208.

Beta C 钛合金在 β 相区的热变形行为及组织演化

许 鑫，董利民，巴宏波，张志强，杨 锐

中国科学院 金属研究所，沈阳 110016

摘 要：利用 Gleeble−3800 热模拟试验机对 beta C 钛合金进行等温压缩试验，研究其在 β 相区的热变形行为。得到了描述热变形行为的本构方程，获得了真应变为 0.7 时的加工图。采用光学显微镜、扫描电子显微镜和电子背散射技术对变形显微组织进行表征。结果表明：流变应力随着应变速率加快而增大，随着试验温度的升高而减小。计算得到的表观激活能为167 kJ/mol，接近β钛的自扩散激活能。加工图和显微组织观察表明在温度为900~1000 °C和变形速率为 0.1~1 s^{-1} 的区间存在一个动态再结晶区。加工图显示，当变形速率大于 1.7 s^{-1} 时，beta C 钛合金发生不稳定变形。Beta C 钛合金在动态再结晶区变形后，经合适的热处理，显微组织可以被优化。

关键词：钛合金；热变形行为；动态再结晶；加工图

(Edited by Xiang-qun LI)